DENTAL MATERIALS 32 (2016) 794–806

Available online at www.sciencedirect.com

ScienceDirect

journal homepage: www.intl.elsevierhealth.com/journals/dema

Combined microcomputed tomography, biomechanical and histomorphometric analysis of the peri-implant bone: a pilot study in minipig model

Matteo Gramanzini[a,b,*,1], *Sara Gargiulo*[a,b,1], *Fernando Zarone*[c], *Rosario Megna*[a], *Antonio Apicella*[d], *Raffaella Aversa*[d], *Marco Salvatore*[e], *Marcello Mancini*[a], *Roberto Sorrentino*[c,d], *Arturo Brunetti*[f,b]

[a] *Institute of Biostructure and Bioimaging, National Research Council, Via T. De Amicis 95, 80145 Naples, Italy*
[b] *CEINGE scarl, Via G. Salvatore 486, 80145 Naples, Italy*
[c] *Department of Neurosciences, Reproductive and Odontostomatological Sciences, School of Medicine, University "Federico II", Via Pansini 5, 80131 Naples, Italy*
[d] *Department of Architecture and Industrial Design, Second University of Naples, Borgo San Lorenzo, 81031 Aversa, Italy*
[e] *IRCCS SDN, Via E. Gianturco 113, 80143 Naples, Italy*
[f] *Department of Advanced Medical Sciences, University "Federico II", Via Pansini 5, 80145 Naples, Italy*

ARTICLE INFO

Article history:
Received 5 October 2015
Received in revised form
9 March 2016
Accepted 22 March 2016

Keywords:
Dental implant
Insertion torque
Resonance frequency analysis
μCT
Histomorphometry
Minipig model

ABSTRACT

Objectives. To present a practical approach that combines biomechanical tests, microcomputed tomography (μCT) and histomorphometry, providing quantitative results on bone structure and mechanical properties in a minipig model, in order to investigate the specific response to an innovative dental biomaterial.

Methods. Titanium implants with innovative three-dimensional scaffolds were inserted in the tibias of 4 minipigs. Primary stability and osseointegration were investigated by means of insertion torque (IT) values, resonance frequency analysis (RFA), bone-to-implant contact (BIC), bone mineral density (BMD) and stereological measures of trabecular bone.

Results. A significant positive correlation was found between IT and RFA ($r = 0.980$, $p = 0.0001$). BMD at the implant sites was 18% less than the reference values ($p = 0.0156$). Peri-implant Tb.Th was 50% higher, while Tb.N was 50% lower than the reference zone ($p < 0.003$) and they were negatively correlated ($r = -0.897$, $p = 0.006$).

* *Corresponding author at*: Institute of Biostructure and Bioimaging, National Research Council, Via T. De Amicis 95, 80145 Naples, Italy. Tel.: +39 0812203401; fax: +39 0812203498.

E-mail addresses: matteo.gramanzini@ibb.cnr.it (M. Gramanzini), sara.gargiulo@ibb.cnr.it (S. Gargiulo), fernandozarone@mac.com (F. Zarone), rosario.megna@ibb.cnr.it (R. Megna), antonio.apicella@unina2.it (A. Apicella), raffaella.aversa@unina2.it (R. Aversa), marsalva@unina.it (M. Salvatore), marcello.mancini@ibb.cnr.it (M. Mancini), errestino@libero.it (R. Sorrentino), brunetti@unina.it (A. Brunetti).

[1] These authors contributed equally to this work.

http://dx.doi.org/10.1016/j.dental.2016.03.025

Significance. μCT increases evaluation throughput and offers the possibility for qualitative three-dimensional recording of the bone–implant system as well as for non-destructive evaluation of bone architecture and mineral density, in combination with conventional analysis methods. The proposed multimodal approach allows to improve accuracy and reproducibility for peri-implant bone measurements and could support future investigations.

1. Introduction

Improvements in bone–implant integration are crucial in modern dental surgery [1,2]. The processes of osseointegration involve an initial mechanical interlocking between alveolar bone and the implant body (primary implant stability) and, later on, a biological fixation through continuous bone apposition (contact osteogenesis) and remodeling toward the implant (secondary implant stability). [3].

Biofidelity is a raising topic in modern medicine; such a concept derives from the study of the biomechanic of tissues and materials and of the biomimetic approach nowadays common in tissue engineering to imitate the properties of natural tissues with bioinspired materials. The bone tissue is as a natural nanostructured biomaterial containing a collagen matrix and hydroxyapatite filler [4]. Tissue engineering using synthetic biomaterials is nowadays used in regenerative therapies and implantology, since they may act as bioactive scaffolds promoting wound healing and bone formation [5]. The physico-chemical and structural characteristics of the scaffold materials have been observed to significantly influence their *in vivo* activity; 3D scaffolds may then represent new clinical applications in bone reconstructive surgery and implantology [6]. In particular, it has been shown that scaffolds made up of porous hydroxyapatite may be colonized by osteoblasts favoring implant stability improvement [7].

Different methods were developed to objectively evaluate implant primary stability. In particular, peak insertion torque (IT) and resonance frequency analysis (RFA) are the parameters that are most globally used and a correlation between primary stability and implant insertion torque has been often suggested in dental literature [8–18]. Insertion torque values were correlated to histological bone-to-implant contact and radiological bone density [19]. RFA is another effective and reliable method to assess implant stability, which positively correlates with IT method [20,21].

The use of patients care newly developed implant materials often requires the use of preclinical models to test their biocompatibility, mechanical stability and safety. Before clinical trials in humans, minipigs are a recommended as animal model for translational research of new dental materials, since their bone structure is similar to that of humans. This species is considered to be closely representative of human bone tissue with regard to morphology [22], bone composition [23], microstructure [24] and remodeling characteristics [25,26]. Moreover, the bone of minipig shows similarities in mineral density and concentration with that of humans [27]. However, minipigs bones have a denser trabecular network: mean cavity path lengths values in the adult man are typically 1200 μm and 350 μm in the minipig [25], while mean trabecular path lengths in child are typically 190 μm and 280 μm in the minipig [28]. Bone regeneration rate in minipigs is comparable to that of humans (namely, 1.2–1.5 mm per day in minipigs and 1.0–1.5 mm per day in humans) [29], and cortical bone mineralization rate is similar to man [30], although mesenchymal stem cells in minipig showed a significantly lower ability than human ones to form differentiated and functional osteoblasts [31]. Based on the above considerations, minipig has been selected in this study as large animal model for the pivotal preclinical testing of our innovative biomaterials and implants. This model would benefit from a non-destructive imaging modality so that mechanical and morphological endpoints can more readily be examined in the same specimens. Presently, microcomputed tomography (μCT) may represent a promising candidate tool for bone characterization when paired to biomechanical testing and standard histology. The implant stability which is critically dependent on structural characteristics and bone quality in a relatively broad area around the implant, may be correlated to bone properties assessed by μCT [32,33]. This technique is fast, precise and, unlike conventional microscopic methods, does not need long time for specimen preparation and it is not impaired by the assessment of a limited number of sections. High-resolution μCT allows measurements of trabecular and cortical bone [34] and a three-dimensional (3D) representation of bone formation at the peri-implant region [35]. In accordance with the principles of the "refinement" and "reduction" declared by Russell and Burch in 1954, μCT allows less use of samples necessary for both biomechanical and morphometric studies. In the present investigation, an innovative hybrid nanocomposite working as a biomimetic scaffold was used to evaluate the performance of the novel material in improving implant primary stability in post-surgical sites.

Our innovative biomaterial appears as a nanoporous transparent glassy polymer (Fig. 1B) able to progressively swell into a hydrogel form (Fig. 1C) when in contact with water solutions (picking up to 30–50% in weight of water), with a kinetic of swelling at 37 °C of about 0.1 mm per hour [36]. The geometrical configuration of the modified implant (Fig. 1A) confines the polymeric scaffold in a niche that allows swelling deformation only in the radial implant direction. This radial guided swelling could be used to stabilize the implant in the socket while creating a biomechanically active interface for bone growth [36]. Moreover, the nanoporosity can be modulated to host cells and growth factors. In previous investigations, the material was characterized for physical, chemical and mechanical properties [37]. It showed a bioactive surface with improved osteoblastic adhesion and proliferation and it could be speculated that this feature could promote more effective

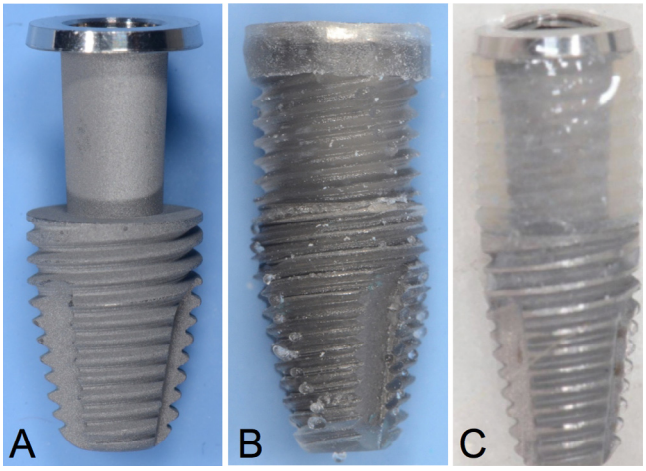

Fig. 1 – (A) Implant prototype, (B) implant with glassy polymer scaffold, and (C) implant with swollen scaffold.

and rapid osseointegration. Furthermore, the finite element analysis (FEA) was used to evaluate the scaffold interactions between the swollen interface and the bone [36]. The elastic modulus of the scaffolds in the swollen state was reported to range between 2 and 10 MPa, which is comparable to that of the periodontal ligament (2–50 MPa) [38–40]. The scaffold had to play two biomechanical functions: a structural one, as part of the fixture, and a bioactive one, as bone growth stimulus. Physiologically, the stresses and deformations induced by the stretching of the periodontal ligament acts as a biomechanical stimulus that favors new bone apposition in the tooth socket [36]. Since the elastic modulus of the swollen scaffold was comparable to that of the periodontal ligament, the FEA confirmed that the swelling of the nanocomposite could act as a biomechanical bone growth input [36]. According to Frost's law regarding the strain dependent adaptive properties of bone [41], the strain values recorded at the bone-scaffold interface fell within the adapted window and were compatible with an organized bone growth. The purpose of this pilot study was to examine the utility of μCT for evaluating bone–implant integration in a minipig model, as an adjunct to conventional histomorphometry and biomechanical testing. The presented approach can serve as a model for future investigations to study implants of different composition or shape with complementary μCT analysis. The null hypothesis stated that there was no association between the biomechanical, histomorphometric and μCT study variables of control and experimental implant sites.

2. Materials and methods

2.1. *Surgical procedures*

All experimental procedures have complied with the Italian D.L. no 116 of 1992 and associated guidelines in the European Communities Council Directive of the 24th of November 1986 (86/609/ECC). Titanium implants (Winsix Implant System, Biosafin, Ancona, Italy) modified with 3D scaffolds were used.

The proposed biomaterial was a hydrophilic hybrid composite made up of nanoinclusions of hydroxyapatite dipped in a ceramo-polymeric matrix composed by polyhydroxylethylmethacrylate and fumed nanosilica.

The scaffolds were designed using a reverse engineering approach and were retained by modified implant prototypes. Standard titanium implants with a diameter of 5.2 mm, a length of 13 mm and a hexagonal internal connection were used. An implant was imported in a solid modeler and meshed to discretize its geometry. Then, a finite element modeling was used to modify the fixture and create the experimental prototype, whose shape was suitable to incorporate the scaffold (Fig. 1A). The coronal part of the screw thread was removed so as to incorporate the scaffold, that had a length of 5 mm and the shape of a truncated cone with the major base apically (major base 0.6 mm, minor base 0.4 mm). The titanium implant prototypes had a micro-rough surface that was acid etched (Fig. 1A).

A steel cylinder was used as tray for the fabrication of the modified implants. A double impression technique was performed using putty and light silicon impression materials. First, the shape of a standard unmodified implant was impressed in the silicon to obtain the external profile shape mold. Subsequently, the modified titanium implant prototypes were inserted in the silicon molds by means of an implant holder and the unpolymerized novel material liquid composite resin [36,37] was injected in the empty space between the external shape mold and the modified implant. The material was let to self-polymerize at room temperature for 15 min. Then, the implant threads were thoroughly polished by means of silicon rubbers. Although, the new biomaterial was designed as self-setting at room temperature, an additional thermal treatement at 80 °C was added to the fabrication procedures in order to favor complete polymerization and stabilization of the scaffolds in their highly rigid glassy state (with an elastic modulus comparable to that of the bone) [36,37] before the surgical insertion (Fig. 1B). The scaffolded implants were then sterilized by means of gamma-rays. The scaffolded implants were introduced unicortically into the left and right proximal tibial metaphysis of 4 male Yucatan minipigs (>18-month old, average body weight 65 kg) with an inter-implant distance of 5–9 mm. The implants were inserted flush with the cortical bone, so as the scaffolds could interface with both the cortical and the spongy bone (Fig. 2). This was made to evaluate if the different elasticity of the bony tissues could affect the swelling of the scaffolds. The animals were sedated by an intramuscular injection (10 mg/kg) of ketamine (Inoketam 1000®, Virbac S.r.l., Milan, Italy) and 0.5 mg/kg midazolam PHG (Hospira, Lake Forest, IL, USA). Anesthesia was induced by mask and, after endotracheal intubation, the minipigs were maintained in spontaneously breathing by inhalation of 3% isoflurane and oxigen. The surgical fields were shaved and disinfected with benzoxonium chloride (Citrosil®, Manetty & Roberts, Milan, Italy). The tibias were exposed by skin incisions and fascial-periosteal flaps. The implant sites were prepared using drills with increasing diameter and a torque-controlled handpiece implant unit at a rotation speed of 25–30 RPM, with continuous external sterile saline irrigation to minimize bone damage caused by overheating. Thereafter, 4 implants were

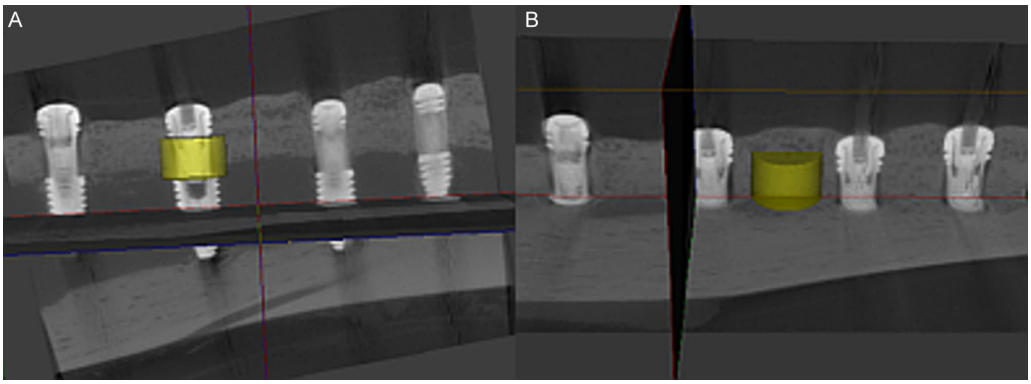

Fig. 2 – Representative sagittal μCT slice showing scaffold-implants systems inserted into the tibia of minipigs after 8 weeks of healing time and the cylindrical volumetric region of interest (VOI), where measurements in peri-implant bone were made (A), at the level of the test zone and (B), at the level of reference zone.

placed in each tibia, according to local anatomy and bone quality. A total of 28 scaffolded fixtures was inserted in 7 tibias; 1 tibia was not used because of unfavorable local anatomy. The insertion torque values were recorded using an electronic torque-control implant handpiece. The implant position was checked by means of radiographs and intensification of brilliance, in order to verify that the scaffolds were in the transition area between the cortical and the spongy bone. The skin and the fascia-periosteum were closed in separate layers with synthetic monofilament non absorbable polypropylene suture (Prolene® 2-0, Ethicon, Somerville, NJ, USA) and a single absorbable suture (Vicryl® 3-0, Ethicon, Somerville, NJ, USA), respectively. Perioperatively, the animals received enrofloxacin 2.5 mg/kg/12 h (Baytril®, Bayer, Barmen, Germany) as antibiotic for 6 days and ketorolac 1 mg/kg/24 h as anti-inflammatory medication for 3 days. The animals were inspected after the first few postoperative days for signs of wound dehiscence or infection and, thereafter, weekly to assess general health. The animals did not show signs of physical impairments and were in stable condition throughout the study. After 8 weeks, animals were sacrificed and specimens containing the implants were fixed in 10% pH 7.0-buffered formalin.

2.2. *Biomechanical analysis*

Insertion torque values (N cm) were recorded during implant placement by means of a torque-controlled implant handpiece. Moreover, once implant placement was completed, a RFA was performed using a dedicated electronic device (Osstell ISQ, Osstell AB, Göteborg, Sweden). The values of resonance frequency were recorded as an implant stability quotient (ISQ) in order to allow a comparison of primary stability between different fixtures [42–44].

2.3. *μCT and 3D reconstruction*

The bone surrounding the implant scaffolds was examined using μCT (eXplore Locus, GE Healthcare, London, Canada). The detector of such μCT system was made up of 2 components, a scintillator and a CCD camera, which were connected with optical fibers. The scintillator is a thin screen of cesium iodide, that luminesces when exposed to X-rays. The camera behind it records the image that is projected onto the scintillator. The projection is saved in digital format. A total of 466 μCT slices, with a pixel size of 45 μm, were imaged at an X-ray energy level of 80 kVp and a current of 450 μA. Exposure time was 100 ms with a total scanning time of 11 min. Images were reconstructed using a modified Feldkamp algorithm and scaled into Hounsfield units (HU). A calibration standard, containing a compartment with 1073 mg/cm^3 SB3 (an epoxy based bone-mimicking material), was used for bone mineral density (BMD) calibration. All data were evaluated in MicroView, 2.1.2 (GE Healthcare, London, Canada). Datasets were resampled to reorient implants perpendicular to the cross-section plane. Before segmentation, threshold levels for bone, implant and scaffold were determined, based on visual inspection of the complete slices and on the gray-scale histogram. The upper and lower threshold levels for bone, implants and scaffold were determined in all 7 samples and did not overlap, allowing to make a clear distinction. An automatic segmentation technique, that utilizes the Otsu method, was used for calculate the value to be used as the threshold to extract the bone from the surrounding structures. The means were calculated and used for each sample. The inter- and intra-examiner variabilities within 1 standard deviation were calculated. Then, a cylindrical, volumetric region of interest (VOI) was placed in correspondence of the scaffold element of the implant circumferentially expanded 2.5 mm around the scaffold, including both cortical and cancellous bone (Fig. 2C), which was defined as the test zone (Fig. 3A). Subsequently, bone, implant and scaffold in the ROI were differentiated based on their threshold levels. Outcome variables were: BMD (mg/cm^3) and bone mineral concentration (BMC, mg); bone volume fraction (BVF), being the % of the ROI which includes bone; bone volume (BV), being the mm^3 of bone that is present in the region of interest; the ratio of the volume of bone present (BV) to the total volume (TV) of interest (%); the ratio of the surface (BS) to the volume (BV) of bone (mm^{-1}); the average trabecular thickness (Tb.Th, mm); the mean trabecular number (Tb.N, mm^{-1}); the mean diameter to the marrow spaces (Tb.Sp, mm). These values were also measured in VOI at an equivalent distance between 2

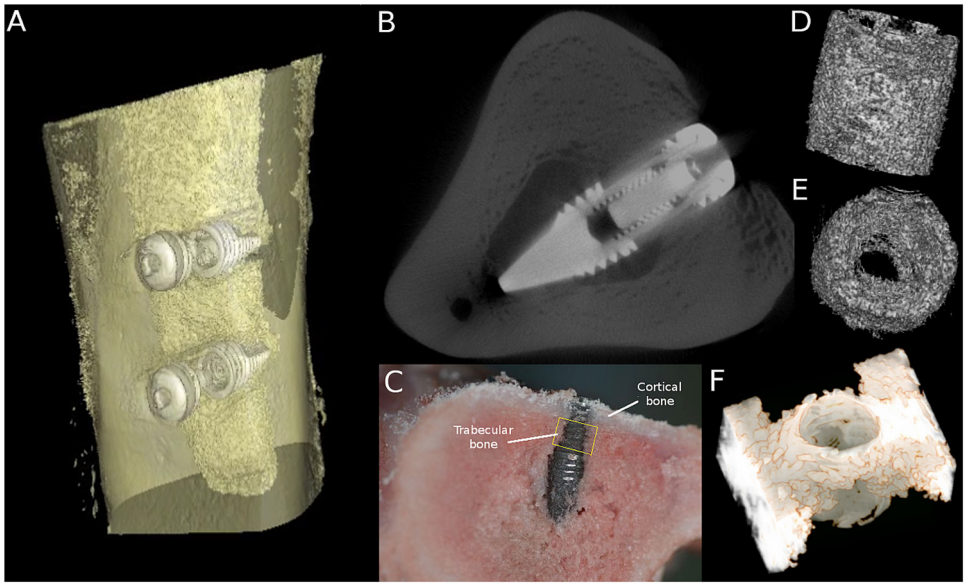

Fig. 3 – (A) High-resolution μCT 3-D volume rendering of minipig tibias with implants. (B) Representative axial μCT image of minipig tibias with implant–bone interface visualization. (C) Representative photograph of minipig tibias with implant position visualization. (D and E) High-resolution μCT 3-D volume rendering of scaffold. (F) High-resolution μCT 3-D volume rendering peri-implant bone.

median implants, as reference zone (Fig. 3B). 3-D volume rendering images were performed on 27 μm μCT dataset using Osirix Imaging Software 5.8.5 (Pixmeo, Bermex, Switzerland) (Fig. 2A, B, E, F).

2.4. *Histology and histomorphometry*

The formalin-fixed specimens were transferred to 70% ethanol solution, dehydrated in ascending concentration of ethanol up to 100%, and then infiltrated and embedded in a hydrophilic acrylic resin (LR White, London Resin Company, Berkshire, England). After polymerization, the specimens were sectioned along the longitudinal axis with a high-precision diamond disk at about 100 μm, provided with a custom-built sawing and a grinding apparatus (TT System, TMA2, Grottammare, Italy). A total of 3 sections was obtained for each implant (1 longitudinal central section and 2 sections at a cutting distance of 600 μm). The sections were ground down to about 60 ± 10 μm and stained with acid fuchsine and toluidine blue. The investigation was conducted in a transmitted bright-field and circularly polarized Light Microscope Axiolab (Zeiss Oberchen, Germany) connected to a high-resolution digital camera (FinePix S2 Pro, Fuji Photo Film Co. Ltd, Minato-Ku, Japan). A histomorphometric software package with image capturing capabilities (Image-Pro Plus 6.0, Media Cybernetics Inc, Bethesda, MD, USA) was used. To ensure accuracy, the software was calibrated for each experimental image using a feature named "Calibration Wizard", which creates a linear remapping of the pixel numbers. The unit of measurement was the pixel. The analyzed parameter was the bone-to-implant contact (BIC, %), defined as the ratio between the length of the scaffold material section in contact with bone and the perimeter of the scaffold area, at 25× magnification. At each measurement, the software was calibrated using the length of the implant as reference. Measurements were performed by a single experienced and calibrated operator. Intra-examiner variability was controlled by carrying out 2 measurements; if the difference between the 2 values was greater than 5%, the measuring was repeated.

2.5. *Statistical analyses*

The study variables were divided into 4 groups as follows: biomechanical (IT and RFA), histomorphometric (BIC), μCT of implant sites (BMD, BMC, BVF, BV, BV/TV, BS/BV, TbTh, TbN, TbSp) and μCT of control sites (cBMD, cBMC, cBVF, cBV, cBV/TV, cBS/BV, cTb/Th, cTbN, cTbSp). Mean, standard deviation, median, minimum and maximum values were calculated for all the variables. Normality was tested using Shapiro–Wilk test and variance homogeneity using Bartlett or Levene test. When data were normally distributed and variance homogeneity was met, the variables were compared using one-way analysis of variance (ANOVA). In case of violation of normality or variance homogeneity, Kruskall–Wallis or Mann–Whitney test were performed. The mean values of 21 variables for 7 tibial samples were used for the statistical analysis. The Pearson correlation was performed for all possible pairs of variables, for a total of 210 combinations. The linear regression coefficients were calculated for the 12 pairs of variables found to be correlated. Moreover, IT, RFA, BIC, BMD, BMC, TbTh, TbN and TbSp were analyzed for comparison among implant sites. Sample size required to reach a 5% significance with a 80% power was estimated for Mann–Whitney, Shapiro–Wilk, Anova and Pearson correlation tests. Statistical analysis was performed using R statistical software (version 3.1.2, R Foundation for Statistical Computing, Vienna, Austria) and the level of significance was set at $p < 0.05$ for all tests.

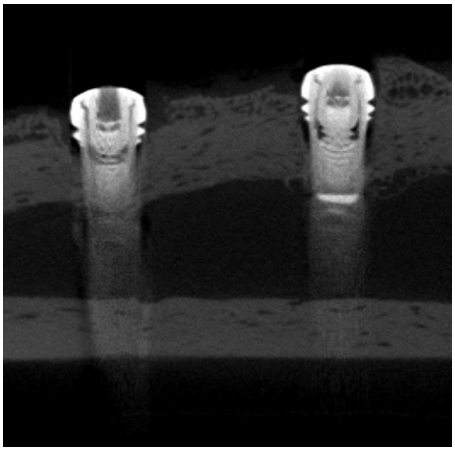

Fig. 4 – Representative sagittal μCT slice showing scaffold-implants systems inserted into the tibia of minipigs after 8 weeks of healing time.

3. Results

The minipigs showed good generale health after surgery and signs of infection were not found at clinical and μCT examination. No effects from X-ray scattering or ring artifacts were found in the μCT images in the peri-implant zone used for measurements (Fig. 4). All the implants were osseointegrated and the peri-implant bone structure consisted of lamellar bone architecture (Fig. 5). The IT and RFA values were reported in Table 1.

According to the results of the present investigation, the null hypothesis was rejected.

Descriptive statistics for biomechanical, μCT and histologic variables were summarized in Table 2. The mean and standard deviation of lower and upper threshold gray-levels for titanium implants, for ceramo-polymeric scaffolds and for bone made by 2 independent and calibrated operators were summarized in Table 3. The first box of Table 2 shows the values of the 3 series of repeated measures for each bone sample; the second box those of all samples for each series of measurements; the third one the global threshold value for implant, scaffold and bone. The inter- and intra-examiner variabilities were equivalent within 1 standard deviation. ANOVA did not reveal differences among the implant sites for BIC ($F = 1.76$, $p = 0.112$) and IT ($F = 2.580$, $p = 0.058$), unlike RFA (Kruskall–Wallis, $p = 0.0156$). For μCT parameters, significant differences were found among the implant sites for BMC ($F = 5.201$, $p = 0.003$) and BMD (Kruskall–Wallis, $p = 0.037$), unlike for TbTh ($F = 2.61$, $p = 0.056$), TbN (Kruskall–Wallis, $p = 0.037$) and TbSp ($F = 1.764$, $p = 0.167$). For comparisons between implant and control sites, ANOVA did not reveal differences between the μCT pairs of variables cBMC–BMC ($F = 1.26$, $p = 0.2831$) and cTbSp–TbSp ($F = 8.68$, $p = 0.0514$), whereas cBMD-BMD and cBV–BV were significantly different (Mann–Whitney test: $p < 0.05$). Fifty Pearson correlations were observed with $p < 0.05$, both between variables of the same group that between variables of different groups. The correlation matrix of all correlation coefficients between the set of variables were reported in Table 4.

Relevant correlations were found between IT and RFA variables ($r = 0.980$, $p = 0.0001$); the μCT pairs of variables cBV–BMC ($r = 0.796$, $p = 0.0322$), cBV–BVF ($r = 0.823$, $p = 0.0230$), cBV–BV ($r = 0.826$, $p = 0.0220$), cBV–BS/BV ($r = -0.873$, $p = 0.0103$), cBV–TbTh ($r = 0.830$, $p = 0.0208$), cBV–TbN ($r = -0.778$, $p = 0.0394$), cBVF–TbN ($r = 0.772$, $p = 0.0419$), cBV/TV–TbN ($r = -0.795$, $p = 0.0326$) and cBV/TV–BS/BV ($r = -0.761$, $p = 0.0470$); and between IT–cTbSp and RFA–cTbSp ($r = -0.859$,

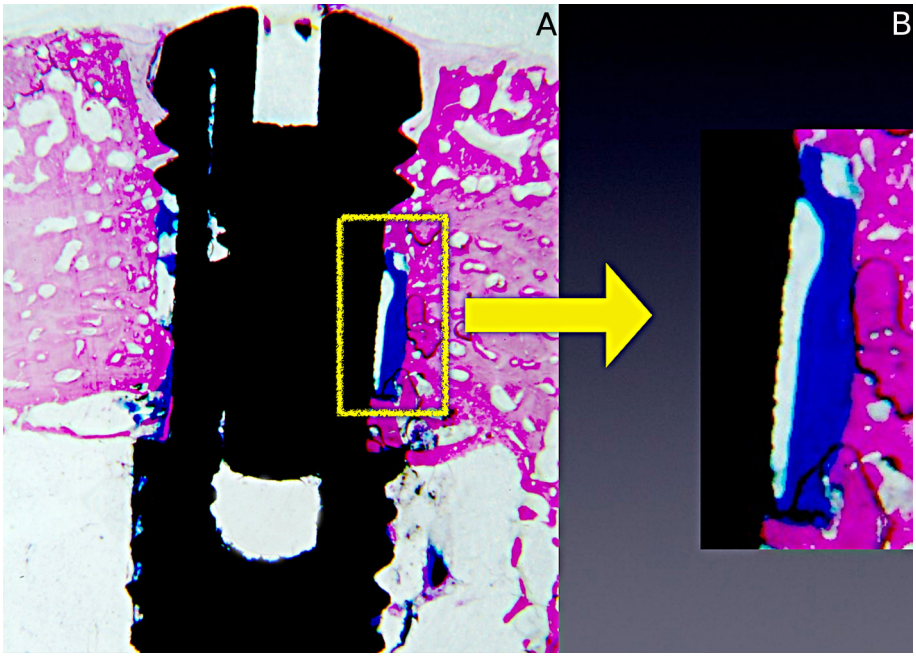

Fig. 5 – (A) Microphotograph of a longitudinal section of a specimen stained with fuchsin acid and toluidine blue. (B) Magnification at 25× to show the contact between scaffold material and bone.

Table 1 – Insertion torque (IT in N cm) and resonance frequency analysis (RFA in ISQ) values of the experimental scaffolded implants.

Minipig	Tibia	Measurement	Implant			
			#1	#2	#3	#4
#1	Left	IT (N cm)	44.2	46.2	47.3	44.5
		RFA (ISQ)	71	73	74	71
	Right	IT (N cm)	48.1	44.6	45.1	44.4
		RFA (ISQ)	75	71	72	71
#2	Left	IT (N cm)	43.4	44.7	42.9	42.5
		RFA (ISQ)	70	71	70	69
	Right	IT (N cm)	51.1	45.2	45.8	44.7
		RFA (ISQ)	79	72	72	71
#3	Left	IT (N cm)	Excluded because of unfavorable local anatomy			
		RFA (ISQ)				
	Right	IT (N cm)	42.0	45.6	42.9	43.1
		RFA (ISQ)	69	72	70	69
#4	Left	IT (N cm)	46.2	43.7	45.2	43.8
		RFA (ISQ)	73	70	72	70
	Right	IT (N cm)	42.6	39.9	43.2	42.2
		RFA (ISQ)	69	66	70	69

Table 2 – Descriptive statistic of sample data.

Variable	Unit	Mean	SD	Min	Median	Max
IT	N cm	44.39	1.63	41.90	43.83	46.70
RFA	ISQ	71.11	1.71	68.50	71.25	73.50
BMD	mg/cm^3	623.7	42.1	533.2	631.9	665.0
BMC	mg	46.62	5.71	36.18	47.47	54.34
BVF	%	0.7809	0.0639	0.6705	0.7925	0.8579
BV	mm^3	74.04	4.42	67.47	73.98	79.39
BV/TV	%	0.8394	0.1118	0.7332	0.8164	1.0743
BS/BV	mm^{-1}	1.641	0.182	1.451	1.634	1.891
TbTh	mm	1.244	0.140	1.058	1.228	1.405
TbN	mm^{-1}	0.6392	0.0335	0.5846	0.6316	0.6866
TbSp	mm	0.3311	0.0744	0.2246	0.3165	0.4351
cBMD	mg/cm^3	764.0	31.5	719.9	765.5	808.9
cBMC	mg	52.40	12.36	33.62	54.13	73.82
cBVF	%	0.6955	0.0983	0.4933	0.7322	0.7799
cBV	mm^3	63.70	12.47	44.50	69.52	73.82
cBV/TV	%	0.7075	0.1009	0.5043	0.7467	0.7913
cBS/BV	mm^{-1}	3.722	1.307	1.923	4.117	5.517
cTbTh	mm	0.6152	0.2675	0.3624	0.4857	1.0399
cTbN	mm^{-1}	1.274	0.355	0.761	1.391	1.617
cTbSp	mm	0.2407	0.0817	0.1507	0.2474	0.3561
BIC	%	76.91	4.17	69.86	77.44	82.34

$p = 0.0134$ and $r = -0.834$, $p = 0.0196$, respectively. A lack of statistical significance was found between the values of BIC and all other variables. Table 5 summarized the linear regression coefficients for the pairs of variables correlated.

4. Discussion

Preclinical research is considered an essential step to test dental materials and implants prior to their clinical use. Minipigs are suitable models for traslational validation due to their anatomical and physiological correspondences with human bone [45]. It is generally accepted that the chemical and physical properties of implant surfaces have a major influence on the structure of the peri-implant bone and thus can improve osseointegration. The scaffolds should work as a medium that offers mechanical properties similar to the host bone, promoting cell adhesion and activity and inducing finally bone growth. The tested innovative nanocomposite material allowed to fabricate stable 3D implant scaffolds that proved to be easy handling and suitable for the surgical procedures. In a previous investigation [36], it was demonstrated that the volumetric expansion of the bioactive novel material due to the swelling of the scaffolds, significantly contributed to the primary stability of the implants. Since it is known that the development of a stable bone–implant interface depends on different factors, it is desirable to use several methods capable to evaluate different bone properties. In this perspective, the integration of biomechanical data, of 3D μCT information and histomorphometric parameters in the same implant/bone

Table 3 – Descriptive statistics for intra-operator and inter-operator reproducibility (mean ± standard deviation).

		OP 1						OP 2					
		Implant		Scaffold		Bone		Implant		Scaffold		Bone	
		LTh	UTh	LTh	UTh	LTh	UTh	LTh	UTh	LTh	UTh	LTh	UTh
Bone sample	#1	4999.3 ± 1.2	13,873.7 ± 1.5	0.3 ± 0.6	1499.3 ± 1.2	1699.0 ± 1.0	4699.0 ± 1.0	4999.3 ± 1.2	13,873.7 ± 1.5	0.3 ± 0.6	1499.7 ± 0.6	1699.0 ± 1.0	4699.0 ± 1.0
	#2	4998.6 ± 1.2	13,872.7 ± 1.2	0.0 ± 0.0	1500.0 ± 0.0	1699.3 ± 0.6	4699.3 ± 0.6	4999.3 ± 1.2	13,872.7 ± 1.2	0.3 ± 0.6	1499.0 ± 1.0	1699.3 ± 0.6	4699.3 ± 0.6
	#3	5000.0 ± 0.0	13,874.7 ± 1.2	0.3 ± 0.6	1499.3 ± 0.6	1698.0 ± 0.0	4694.6 ± 0.6	5000.0 ± 0.0	13,872.7 ± 1.2	0.3 ± 0.6	1499.3 ± 0.6	1694.7 ± 6.7	4694.0 ± 1.0
	#4	4999.0 ± 1.0	13,873.0 ± 1.7	0.3 ± 0.6	1499.6 ± 0.6	1698.3 ± 0.6	4693.6 ± 1.5	4999.0 ± 1.0	13,873.7 ± 1.5	0.0 ± 0.0	1499.6 ± 0.6	1695.7 ± 5.8	4694.3 ± 2.1
	#5	4999.3 ± 1.2	13,873.7 ± 1.5	0.3 ± 0.6	1499.6 ± 0.6	1699.6 ± 0.6	4699.6 ± 0.6	4999.3 ± 1.2	13,873.7 ± 1.5	0.7 ± 0.6	1499.6 ± 0.6	1699.6 ± 0.6	4699.3 ± 0.6
	#6	4999.3 ± 1.2	13,873.0 ± 1.7	0.3 ± 0.6	1499.0 ± 1.0	1699.0 ± 1.0	4699.3 ± 1.2	4999.3 ± 1.2	13,872.7 ± 1.2	0.3 ± 0.6	1499.0 ± 1.0	1699.0 ± 1.0	4699.0 ± 1.0
	#7	4999.3 ± 1.2	13,872.0 ± 1.2	0.3 ± 0.6	1499.3 ± 0.6	1700.0 ± 0.0	4699.7 ± 0.6	4999.3 ± 1.2	13,872.0 ± 1.2	0.3 ± 0.6	14,993 ± 0.6	1700.0 ± 0.0	4699.7 ± 0.6
Repeated measures series	1°	4999.3 ± 0.9	13,874.1 ± 1.1	0.1 ± 0.4	1499.6 ± 0.8	1698.7 ± 1.0	4698.0 ± 2.5	4999.6 ± 0.8	13,873.3 ± 1.3	0.2 ± 0.4	1499.3 ± 0.7	1698.8 ± 0.8	4697.7 ± 2.6
	2°	4999.1 ± 1.0	13,872.7 ± 1.3	0.1 ± 0.4	1499.1 ± 0.7	1698.8 ± 0.7	4698.2 ± 2.6	4999.0 ± 1.1	13,873.0 ± 1.3	0.2 ± 0.4	1499.3 ± 0.5	1697.2 ± 3.8	4697.7 ± 2.4
	3°	4999.4 ± 1.0	13,873.1 ± 1.5	0.6 ± 0.5	1499.7 ± 0.5	1699.8 ± 0.8	4697.4 ± 2.9	4999.4 ± 1.0	13,873.0 ± 1.3	0.7 ± 0.5	1499.5 ± 0.8	1697.7 ± 4.9	4697.2 ± 2.9
Global value		4999.3 ± 1.0	13,873.3 ± 1.4	0.3 ± 0.5	1499.5 ± 0.7	1699.3 ± 0.9	4697.3 ± 2.6	4999.3 ± 0.9	13,873.1 ± 1.2	0.3 ± 0.5	1499.4 ± 0.7	1698.2 ± 3.5	4698.3 ± 2.5

OP: operator; LTh: lower HU threshold; UTh: upper HU threshold.

sample enables to improve evaluation of implant stability. Primary implant stability is considered of paramount importance to achieve osseointegration and IT and RFA values are validated mechanical parameters to evaluate the strenght of the interaction between the host bone and implant surface [46]. In dental literature, minimum IT values for immediate loading ranged from 32 to 50 N cm [8,12,14,47–51], sufficient for retaining micromovements within limits [12,49]. RFA has been used at early stages of osseointegration or in monitoring over time and increases during the healing phase [52]. The acceptable range of RFA, that indicates stability, lies between 55 and 85 ISQ [53–55]. Moreover, IT and ISQ values have shown a positive correlation [33,56]. The measurements of IT and RFA recorded in this study were in the interval of values reported as adequate in literature. In agreement with the literature, a strong correlation between IT and RFA was found. Secondary stability is determined by the new bone formation and remodeling at the implant interface, and greater bone contact is generally believed to result in better implant stability [57]. In the examined samples, lamellar bone was visible in intimate contact with the scaffold surface. The BIC values in this study were found to be appropriate to warrant stability, since they were higher than 50%, the minimum value considered necessary for loading and for ensure long-term survival of implants [58]. Good primary stability may be related to better bone tissue response. However, the formula of higher biomechanical parameters translating into better osseointegration may not always be true, because the quantity and quality of bone may vary significantly among subjects. Despite IT and RFA have been considered valid tools to foresee the bone quality and primary stability of implant sites, their comparison with radiologic or histomorphometric tests gave contradictory results [59–69]. Friberg et al. [61] demonstrated that IT was correlated to histomorphometric BIC and to radiological BMD of the prepared sites [19,52]. Other authors demonstrated that IT values was correlated with BMD of the receiving bone site, obtained by measuring CT or μCT [9,70,71]. In contrast, it has been reported that RFA suffers from a lack of sensitivity to the quality of surrounding bone [72], and a correlation with histomorphometric BIC was not found [56,73]. The biomechanical properties of the bone seems to be related both to its mineral content and microarchitecture [74]. Moreover, bone quality parameters assessed by μCT in peri-implant regions did not seem linearly correlated to biomechanical variables [68]. The present study failed to find a correlation between BIC and biomechanical or μCT parameters. Nevertheless, a strong relationship between IT–cTbSp and RFA–cTbSp was found, where negative values of r indicate that, increasing cTbSp, IT and RFA decreased. Although histology is the most common method for analysing bone formation around implants, it also has limitations. Sample preparation is time consuming, may alter bone–implant interface and a limited number of 2D sections per sample are used for the approximation of mean values of BIC. Conversely, μCT is a non-destructive, fast and precise technique, that provides accurate modeling and analysis of 3D images of bone samples, and can evaluate both qualitative and quantitative morphometry of bone integration around dental implants [57,75]. μCT produces voxels in the range of 5–50 μm, or approximately 1.000 times smaller in volume than clinical CT voxels [76,77]. A wide range of specimens may be examined

Table 4 – Pearson correlation matrix.

	IT	RFA	BIC	TMD	TMC	BVF	BV	BV/TV	BS/BV	TbTh	TbN	TbSp	cTMD	cTMC	cBVF	cBV	cBV/TV	cBS/BV	cTbTh	cTbN
RFA	0.980*																			
BIC	−0.171	−0.286																		
BMD	0.321	0.384	0.108																	
BMC	0.226	0.281	0.123	0.928*																
BVF	0.310	0.352	0.199	0.899*	0.978*															
BV	0.036	0.094	0.206	0.772*	0.941*	0.937*														
BV/TV	−0.093	−0.193	−0.052	−0.775*	−0.535	−0.462	−0.350													
BS/BV	−0.407	−0.467	−0.054	−0.755*	−0.857*	−0.931*	−0.857*	0.290												
TbTh	0.408	0.455	0.107	0.743	0.840*	0.925*	0.838*	−0.268	−0.996*											
TbN	−0.520	−0.596	0.123	−0.527	−0.566	−0.688	−0.564	0.181	0.896*	−0.897*										
TbSp	−0.242	−0.244	−0.297	−0.800*	−0.945*	−0.965*	−0.939*	0.280	0.868*	−0.870*	0.567									
cBMD	−0.249	−0.094	−0.205	0.320	0.491	0.473	0.673	−0.215	−0.552	0.494	−0.480	−0.394								
cBMC	0.071	0.243	−0.463	0.304	0.415	0.410	0.523	−0.221	−0.560	0.492	−0.602	−0.279	0.918*							
cBVF	0.301	0.406	−0.161	0.287	0.465	0.544	0.612	0.003	−0.736	0.695	−0.772*	−0.474	0.794*	0.869*						
cBV	0.327	0.450	−0.081	0.717	0.796*	0.823*	0.826*	−0.452	−0.873*	0.830*	−0.778*	−0.709	0.782*	0.823*	0.864*					
cBV/TV	0.320	0.426	−0.134	0.329	0.492	0.574	0.628	−0.043	−0.761*	0.722	−0.795*	−0.496	0.788*	0.863*	0.998*	0.884*				
cBS/BV	0.294	0.146	0.139	−0.172	−0.299	−0.336	−0.503	0.140	0.505	−0.470	0.566	0.228	−0.921*	−0.840*	−0.751	−0.663	−0.750			
cTbTh	−0.453	−0.292	−0.201	0.157	0.248	0.242	0.432	−0.232	−0.362	0.322	−0.403	−0.124	0.903*	0.795*	0.593	0.561	0.591	−0.968*		
cTbN	0.643	0.501	0.134	−0.037	−0.068	−0.050	−0.233	0.242	0.140	−0.117	0.206	−0.064	−0.719	−0.563	−0.302	−0.294	−0.302	0.854*	−0.941*	
cTbSp	−0.858*	−0.834*	0.066	−0.210	−0.298	−0.390	−0.260	−0.173	0.502	−0.488	0.524	0.402	−0.032	−0.264	−0.587	−0.478	−0.589	−0.087	0.297	−0.585

*$p < 0.05$.

Table 5 – Linear regression coefficients for correlated variables ($y = \alpha^* x + \beta$).

y	x	α	err. st. α	β	err. st. β
IT	RFA	0.930	0.084	−21.73	6.00
cTbSp	IT	−0.043	0.012	2.156	0.512
cTbSp	RFA	−0.040	0.012	3.070	0.837
cBV	TMC	1.739	0.591	−17.39	27.74
cBV	BVF	160.6	49.6	−61.74	38.84
cBV	BV	2.333	0.712	−109.1	52.8
cBV	BS/BV	−59.77	14.92	161.8	24.6
cBV	TbTh	73.82	22.18	−28.15	27.74
cBV	TbN	−289.7	104.6	248.9	66.9
cBVF	TbN	−2.267	0.834	2.144	0.534
cBV/TV	TbN	−2.396	0.818	2.239	0.523
cBV/TV	BS/BV	−0.422	0.161	1.399	0.265

using μCT, including teeth, bone and materials such as ceramics, polymers or biomaterial scaffolds [34]. Although formalin fixation may alter the mechanical properties of bone, several studies showed that it has no effect on the mineral composition of bone [78,79]. Moreover, in a recent study it was reported that formalin fixation and freezing would not adversely affect the viscoelastic and elastic mechanical properties of murine bone [80]. In the present investigation, no artifacts were found in the μCT images in correspondence of the zones around the scaffolds (Fig. 4). However, it is difficult to determine the precise effect of material composition on the image quality. Nevertheless, these limits do not necessarily prevent suitable analysis of peri-implant bone by μCT, even if extensive experimentation for appropriate set up should be performed for each equipment. Moreover, intra- and inter-examiner reproducibility and reliability of threshold levels for methodology validation were compared, with good results. Therefore, this method can be properly used as complement of the established gold standard, allowing a refinement in the planning of experiments with animal models, in accordance with the 3Rs principles, and to improve the quality of future studies. The mean density of the newly formed bone can be an indication of how the remodeling process has been successful in terms of new bone tissue density, similar to the reference areas. In the present study, the entity of osseointegration was visualized and quantified by μCT 3D reconstruction. μCT for preclinical application provides higher spatial resolution than clinical CT, then peri-implant bone measurements at 45 μm resolution could be used as a guide to predict implant integration. In the examined samples, cBV of the reference zone was found correlated with BMC, BV, Tb.N, Tb.Th of the bone surrounding the scaffold. Peri-implant BMD was 18% less than the control value, probably due to the fact that minipigs were sacrificed 8 weeks after implants placement. An adequate healing period for osseointegration in humans is assumed to be 12 weeks [81] and bone formation and remodeling in minipigs have been estimated to be approximately comparable to those of humans [29]. In minipigs, an healing period of 4 weeks is considered short [82] and histological evaluation of bone density demonstrated an increase of mean values over time at 4, 8 and 12 weeks after receiving different types of dental implants [83]. Nevertheless, in this study an interval of reference values for mineral density of peri-implant bone was defined after the widely adopted healing period of 8 weeks in minipigs, corresponding to the desirable values of the biomechanical properties. Bone in the vicinity of the implants showed evidence of an increase of 50% in trabecular thickness but a similar decrease of their number when compared to the bone in the control zone ($p = 0.0021$). It is likely that these changes in trabecular microarchitecture parameters may be a way for low density bone to respond to the stress induced by loading, since bone strength increases proportionally to the square of the trabecular radius [84]. In some studies, bone density were measured preoperatively in implant recipient site of human patients by clinical CT and were recorded in Hounsfield units (HU) or converted in mg/cm^3 using a calibration phantom with known density values [19,46,66–68]. As to bone density analysis, the method using BMD calibration standard is more accurately compared with the method with Hounsfield units [85]. Bilhan et al. [86] reported in an *ex vivo* study that HU values assessed by clinical CT could be a misleading tool for the determination of bone density and could result in an overestimation of micro-architectural parameters, while μCT, with a spatial resolution not more than 100 μm, was able to reasonably evaluate bone quantitatively and qualitatively with a good correlation between histomorphometric and microtomographic data [85]. The main limitation of this proof of concept study was the relatively small number of samples. Thus, caution is required in the interpretation of the results. Estimated sample sizes per group ranged from 11 for Pearson correlation tests to 26 for Anova. Further studies in a larger group of animals are needed to assess the sensitivity of this approach that combines biomechanical tests, microcomputed tomography (μCT) and histomorphometry to improve evaluation of implant stability.

5. Conclusion

In conclusion, the results from this pilot study showed the feasibility and usefulness of μCT imaging in the characterization of bone density and microarchitecture to predict structural changes in minipig bone undergoing new biomaterials and implants, in a complementary way to the common biomechanical testing and hystomorphometry. The innovative hybrid ceramopolymeric nanocomposite was effective in fabricating three-dimensional bioactive scaffolds. Further clinical studies are needed to confirm that the experimental nanocomposite could be useful for ensuring scaffold fixation

avoiding micromotion at the tissue/biomaterial interface, promoting accelerated implant osseointegration and loading.

Conflict of interest

The authors declare that there is no conflict of interest.

Author contributions

- **Matteo Gramanzini**: conception and design of the work; acquisition, analysis and interpretation of data; imaging data reconstruction and post-processing; critical revision of data and statistics; drafting article.
- **Sara Gargiulo**: conception and design of the work; acquisition, analysis and interpretation of data; imaging data reconstruction and post-processing; critical revision of data and statistics; drafting article.
- **Roberto Sorrentino**: conception and design of the work; acquisition, analysis and interpretation of data; critical revision of article.
- **Rosario Megna**: statistics; analysis and interpretation of data; critical revision of article.
- **Antonio Apicella**: conception and design of the work; analysis and interpretation of data.
- **Raffaella Aversa**: acquisition, analysis and interpretation of data; critical revision of article.
- **Marco Salvatore**: critical revision of article and final approval; analysis and interpretation of data.
- **Marcello Mancini**: critical revision of article and final approval; analysis and interpretation of data.
- **Fernando Zarone**: conception and design of the work; critical revision of article and final approval.
- **Arturo Brunetti**: conception and design of the work; critical revision of article and final approval.

Acknowledgements

The authors would like to thank Prof. Enrico Felice Gherlone and his team of the University Vita Salute San Raffaele of Milan (Italy) for the support in histological and histomorphometrical analyses and Biosafin (Ancona, Italy) for the technical support providing the implant prototypes of the Winsix Implant System.

REFERENCES

[1] Franchi M, Fini M, Martini D, Orsini E, Leonardi L, Ruggeri A, et al. Biological fixation of endosseous implants. Micron 2005;36:665–71.
[2] Joos U, Wiesmann HP, Szuwart T, Meyer U. Mineralization at the interface of implants. Int J Oral Maxillofac Surg 2006;35:783–90.
[3] Berglundh T, Abrahamsson I, Lang NP, Lindhe J. De novo alveolar bone formation adjacent to endosseous implants. Clin Oral Implants Res 2003;14:251–62.
[4] Otsuka M, Nakagawa H, Otsuka K, Ito A, Higuchi WI. Effect of geometrical structure on the in vivo quality change of a three-dimensionally perforated porous bone cell scaffold made of apatite/collagen composite. J Biomed Mater Res B Appl Biomater 2013;101:338–45.
[5] Panseri S, Russo A, Sartori M, Giavaresi G, Sandri M, Fini M, et al. Modifying bone scaffold architecture in vivo with permanent magnets to facilitate fixation of magnetic scaffolds. Bone 2013;56:432–9.
[6] Velasquez P, Luklinska ZB, Meseguer-Olmo L, Mate-Sanchez de Val JE, Delgado-Ruiz RA, Calvo-Guirado JL, et al. αTCP ceramic doped with dicalcium silicate for bone regeneration applications prepared by powder metallurgy method: in vitro and in vivo studies. J Biomed Mater Res A 2013;101:1943–54.
[7] Vozzi G, Corallo C, Carta S, Fortina M, Gattazzo F, Galletti M, et al. Collagen–gelatine–genipin–hydroxyapatite composite scaffolds colonized by human primary osteoblasts are suitable for bone tissue engineering applications: in vitro evidences. J Biomed Mater Res Part A 2013;00A.
[8] Calandriello R, Tomatis M, Rangert B. Immediate functional loading of Bra°nemark system implants with enhanced initial stability: a prospective 1- to 2-year clinical and radiographic study. Clin Implant Dent Relat Res 2003;5:10–20.
[9] Beer A, Gahleitner A, Holm A, Tschabitscher M, Homolka P. Correlation of insertion torques with bone mineral density from dental quantitative CT in the mandible. Clin Oral Implants Res 2003;14:616–20.
[10] Meredith N. Assessment of implant stability as a prognostic determinant. Int J Prosthodont 1998;11:491–501.
[11] O'Sullivan D, Sennerby L, Meredith N. Measurements comparing the initial stability of five designs of dental implants: a human cadaver study. Clin Implant Dent Relat Res 2000;2:85–92.
[12] Nikellis I, Levi A, Nicolopoulos C. Immediate loading of 190 endosseous dental implants: a prospective observational study of 40 patients treatments with up to 2-years data. Int J Oral Maxillofac Implants 2004;19:116–23.
[13] Friberg B, Sennerby L, Gröndahl K, Bergström C, Bäck T, Lekholm U. On cutting torque measurements during implant placement: a 3 years clinical prospective study. Clin Implant Dent Relat Res 1999;1:75–83.
[14] Hui E, Chow J, Li D, Liu J, Wat P, Law H. Immediate provisional single-tooth implant replacement with Bra°nemark 612 system: preliminary report. Clin Implant Dent Relat Res 2001;3:79–86.
[15] Johansson P, Strid KG. Assessment of bone quality from cutting placement resistance during implant surgery. Int J Oral Maxillofac Implants 1994;9:279–88.
[16] Lorenzoni M, Pertl C, Zhang K, Wimmer G, Wegscheider WA. Immediate loading of single-tooth implants in the anterior maxilla. Preliminary results after one year. Clin Oral Implants Res 2003;14:180–7.
[17] Shalabi MM, Wolke JGC, Jansen JA. The effects of implant surface roughness and surgical technique on implant fixation in an *in vitro* model. Clin Oral Implants Res 2006;17:172–8.
[18] Sakoh J, Wahlmann U, Stender E, Nat R, Al-Nawas B, Wagner W. Primary stability of a conical implant and a hybrid, cylindric screw-type implant in vitro. Int J Oral Maxillofac Implants 2006;21:560–6.
[19] Friberg B, Sennerby L, Roos J, Johansson P, Strid CG, Lekholm U. Evaluation of bone density using cutting resistance measurements and microradiography. Clin Oral Implants Res 1995;6:164–71.
[20] Degidi M, Perrotti V, Strocchi R, Piattelli A, Iezzi G. Is insertion torque correlated to bone–implant contact percentage in the early healing period? A histological and

histomorphometrical evaluation of 17 human-retrieved dental implants. Clin Oral Implants Res 2009;20:778–81.
[21] Degidi M, Daprile G, Piattelli A. Primary stability determination by means of insertion torque and RFA in a sample of 4,135 implants. Clin Implant Dent Relat Res 2010;21:213–20.
[22] Thorwarth M, Schultze-Mosgau S, Kessler P, Wiltfang J, Schlegel KA. Bone regeneration in osseous defects using a resorbable nanoparticular hydroxyapatite. J Oral Maxillofac Surg 2005;63:1626–33.
[23] Mosekilde L, Kragstrup J, Richards A. Compressive strength, ash weight, and volume of vertebral trabecular bone in experimental fluorosis in pigs. Calcif Tissue Int 1987;40:318–22.
[24] Martiniakova M, Grosskopf B, Omelka R, Vondráková M, Bauerová M. Differences among species in compact bone tissue microstructure of mammalian skeleton: use of a discriminant function analysis for species identification. J Forensic Sci 2006;51:1235–9.
[25] Mosekilde L, Weisbrode SE, Safron JA, Stills HF, Jankowsky ML, Ebert DC, et al. Calcium-restricted ovariectomized Sinclair S-1 minipigs: an animal model of osteopenia and trabecular plate perforation. Bone 1993;14:379–82.
[26] Martınez-Gonzalez JM, Cano-Sanchez J, Campo-Trapero J, Gonzalo-Lafuente JC, Díaz-Regañón J, Vázquez-Piñeiro MT. Evaluation of minipigs as an animal model for alveolar distraction. Oral Surg Oral Med Oral Pathol Oral Radiol Endod 2005;99:11–6.
[27] Aerssens J, Boonen S, Lowet G, Dequeker J. Interspecies differences in bone composition, density, and quality: potential implications for in vivo bone research. Endocrinology 1998;139:663–70.
[28] Beddoe HA. Quantitative study of the structure of trabecular bone in man, rhesus monkey, beagle and miniature pig. Calcif Tissue Res 1978;25:273–81.
[29] Laiblin C, Jaeschke G. Clinical chemistry examinations of bone and muscle metabolism under stress in the Gottingen miniature pig—an experimental study. Berl Munch Tierarztl Wochenschr 1979;92:124–8.
[30] Kragstrup J, Richards A, Fejerskov O. Effects of fluoride on cortical bone remodeling in the growing domestic pig. Bone 1989;10:421–4.
[31] Heino Terhi J, Alm JJ, Moritz N, Aro HT. Comparison of the osteogenic capacity of minipig and human bone marrow-derived mesenchymal stem cells. J Orthop Res 2012;30:1019–25.
[32] Homolka P, Beer A, Birkfellner W, Nowotny R, Gahleitner A, Tschabitscher M, et al. Bone mineral density measurement with dental quantitative CT prior to dental implant placement in cadaver mandibles: pilot study. Radiology 2002;224:247–52.
[33] Turkyilmaz I, McGlumphy EA. Influence of bone density on implant stability parameters and implant success: a retrospective clinical study. BMC Oral Health 2008;8:32, http://dx.doi.org/10.1186/1472-6831-8-32.
[34] Swain MV, Xue J. State of the art of micro-CT applications in dental research. Int J Oral Sci 2009;1:177–88.
[35] Park YS, Yi KY, Lee IS, Yung YC. Correlation between microtomography and histomorphometry for assessment of implant osseointegration. Clin Oral Implants Res 2005;16:156–60.
[36] Aversa R, Sorrentino R, Apicella A. New biomimetic hybrid nanocomposites for early fixation prostheses. Adv Mater Res 2015;1088:487–94.
[37] Schiraldi C, D'agostino A, Oliva A, Flamma F, De Rosa A, Apicella A, Aversa R, De Rosa M. Development of hybrid materials based on hydroxyethylmethacrylaye as supports for improving cell adhesion and proliferation. Biomaterials 2004;25:3645–53.
[38] Natali AN, Pavan PG, Scarpa C. Numerical analysis of tooth mobility: formulation of a non-linear constitutive law for the periodontal ligament. Dent Mater 2004;22:3–22, 9.
[39] Colin SS, Wiskott HWA, Justiz J, Botsis J, Belser UC. In vitro time-dependent response of periodontal ligament to meachanical loading. J Appl Physiol 2005;99:2369–78.
[40] Aversa R, Apicella D, Perillo L, Sorrentino R, Zarone F, Ferrari M, Apicella A. Non-linear elastic three-dimensional finite element analysis on the effect of endocrown material rigidity on alveolar bone remodeling process. Dent Mater 2009;25:678–90.
[41] Frost HM. Bone mass and the mechanostat: a proposal. Anat Rec 1987;219:1–9.
[42] Calvo-Guirado JL, Gómez-Moreno G, Delgado-Ruiz RA, Maté Sánchez de Val JE, Negri B, Ramírez Fernández MP. Clinical and radiographic evaluation of osseotite-expanded platform implants related to crestal bone loss: a 10-year study. Clin Oral Implants Res 2014;25:352–8.
[43] Romanos GE, Ciornei G, Jucan A, Malmstrom H, Gupta B. In vitro assessment of primary stability of straumann® implant designs. Clin Implant Dent Relat Res 2014;16:89–95.
[44] Salimov F, Tatli U, Kürkçü M, Akoğlan M, Oztunç H, Kurtoğlu C. Evaluation of relationship between preoperative bone density values derived from cone beam computed tomography and implant stability parameters: a clinical study. Clin Oral Implants Res 2014;25:1016–21.
[45] Wang S, Liu Y, Fang D, Shi S. The miniature pig: a useful large animal model for dental and orofacial research. Oral Dis 2007;13:530–7.
[46] Degidi M, Daprile G, Piattelli A, Iezzi G. Development of a new implant primary stability parameter: insertion torque revisited. Clin Implant Dent Relat Res 2013;15:637–44.
[47] Hui E, Chow J, Li D, Liu J, Wat P, Law H. Immediate provisional single-tooth implant replacement with Bra°nemark system: preliminary report. Clin Implant Dent Relat Res 2001;3:79–86.
[48] Malo P, Rangert B, Dvarsater L. Immediate function of Bra°nemark implants in the esthetic zone: a retrospective clinical study with 6 months to 4 years of follow-up. Clin Implant Dent Relat Res 2000;2:138–46.
[49] Horiuchi K, Uchida H, Yamamoto K, Sugimura M. Immediate loading of Branemark system implants following placement in edentulous patients: a clinical report. Int J Oral Maxillofac Implants 2000;15:824–30.
[50] Ottoni JM, Oliveira ZF, Mansini R, Cabral AM. Correlation between placement torque and survival of single-tooth implants. Int J Oral Maxillofac Implants 2005;20:769–76.
[51] Neugebauer J, Traini T, Thams U, Piattelli A, Zöller JE. Peri-implant bone organization under immediate loading state. Circularly polarized light analyses: a minipig study. J Periodontol 2006;77:152–60.
[52] Meredith N, Book K, Friberg B, Jemt T, Sennerby L. Resonance frequency measurements of implant stability in vivo. A cross-sectional and longitudinal study of resonance frequency measurements on implants in the edentulous and partially dentate maxilla. Clin Oral Implants Res 1997;8:226–33.
[53] Meredith N, Rasmussen L, Sennerby L, Alleyne D. Mapping implant stability by resonance frequency analysis. Med Sci Res 1996;24:191–3.
[54] Meredith N, Alleyne D, Cawley P. Quantitative determination of the stability of the implant-tissue interface using resonance frequency analysis. Clin Oral Implants Res 1996;7:261–7.
[55] Sennerby L, Meredith N. Implant stability measurements using resonance frequency analysis: biological and

biomechanical aspects and clinical implications. Periodontology 2000 2008;47:51–66.
[56] Dagher M, Mokbel N, Jabbour G, Naaman N. Resonance frequency analysis, insertion torque, and bone to implant contact of 4 implant surfaces: comparison and correlation study in sheep. Implant Dent 2014;23:672–8.
[57] Park YS, Yi KY, Lee IS, Jung YC. Correlation between microtomography and histomorphometry for assessment of implant osseointegration. Clin Oral Implants Res 2005;16:156–60.
[58] Roberts WE. Bone tissue interface. J Dent Educ 1988;52:804–9.
[59] Turkyilmaz I. A comparison between insertion torque and resonance frequency in the assessment of torque capacity and primary stability of Brånemark system implants. J Oral Rehabil 2006;33:754–9.
[60] Alsaadi G, Quirynen M, Michiels K, Jacobs R, van Steenberghe D. A biomechanical assessment of the relation between the oral implant stability at insertion and subjective bone quality assessment. J Clin Periodontol 2007;34:359–66.
[61] Friberg B, Sennerby L, Roos J, Lekholm U. Identification of bone quality in conjunction with insertion of titanium implants. Clin Oral Implants Res 1995;6:213–9.
[62] Turkyilmaz I, Tumer C, Ozbek EN, Tözüm TF. Relations between the bone density values from computerized tomography, and implant stability parameters: a clinical study of 230 regular platform implants. J Clin Periodontol 2007;34:716–22.
[63] Nkenke E, Hahn M, Weinzierl K, Radespiel-Tröger M, Neukam FW, Engelke K. Implant stability and histomorphometry: a correlation study in human cadavers using stepped cylinder implants. Clin Oral Implants Res 2003;14:601–9.
[64] da Cunha HA, Francischone CE, Filho HN, de Oliveira RC. A comparison between cutting torque and resonance frequency in the assessment of primary stability and final torque capacity of standard and TiUnite single-tooth implants under immediate loading. Int J Oral Maxillofac Implants 2004;19:578–85.
[65] Schliephake H, Sewing A, Aref A. Resonance frequency measurements of implant stability in the dog mandible: experimental comparison with histomorphometric data. Int J Oral Maxillofac Surg 2006;35:941–6.
[66] Ito Y, Sato D, Yoneda S, Ito D, Kondo H, Kasugai S. Relevance of resonance frequency analysis to evaluate dental implant stability: simulation and histomorphometrical animal experiments. Clin Oral Implants Res 2008;19:9–14.
[67] Miyamoto I, Tsuboi Y, Wada E, Suwa H, Iizuka T. Influence of cortical bone thickness and implant length on implant stability at the time of surgery – clinical, prospective, biomechanical, and imaging study. Bone 2005;37:776–80.
[68] Huwiler MA, Pjetursson BE, Bosshardt DD, Salvi GE, Lang NP. Resonance frequency analysis in relation to jawbone characteristics and during early healing of implant installation. Clin Oral Implants Res 2007;18:275–80.
[69] Scarano A, Degidi M, Iezzi G, Petrone G, Piattelli A. Correlation between implant stability quotient and bone–implant contact: a retrospective histological and histomorphometrical study of seven titanium implants retrieved from humans. Clin Implant Dent Relat Res 2006;8:218–22.
[70] Homolka P, Beer A, Birkfellner W, Nowotny R, Gahleitner A, Tschabitscher M, Bergmann H. Bone mineral density measurement with dental quantitative CT prior to dental implant placement in cadaver mandibles: pilot study. Radiology 2002;224:247–52.
[71] Rebaudi A, Laffi N, Benedicenti S, Angiero F, Romanos GE. Microcomputed tomographic analysis of bone reaction at insertion of orthodontic mini-implants in sheep. Int J Oral Maxillofac Implants 2011;26:1233–40.
[72] Östman PO, Hellman M, Wendelhag I, Sennerby L. Resonance frequency analysis measurements of implants at placement surgery. Int J Prosthodont 2006;19:77–83.
[73] Meredith N, Shagaldi F, Alleyne D, Sennerby L, Cawley P. The application of resonance frequency measurements to study the stability of titanium implants during healing in the rabbit tibia. Clin Oral Implants Res 1997;8:234–43.
[74] Majumdar S, Kothari M, Augat P, Newitt DC, Link TM, Lin JC, et al. High-resolution magnetic resonance imaging: three-dimensional trabecular bone architecture and biomechanical properties. Bone 1998;22:445–54.
[75] Müller B, Bernhardt R, Weitkamp T, Beckmann F, Bräuer R, Schurigt U, et al. Morphology of bony tissues and implants uncovered by high-resolution tomographic imaging. Int J Mater Res 2007;98:613–21.
[76] Feldkamp LA, Goldstein SA, Parfitt AM, Jesion G, Kleerekoper M. The direct examination of three-dimensional bone architecture in vitro by computed tomography. J Bone Miner Res 1989;4:3–11.
[77] Kuhn JL, Goldstein SA, Feldkamp LA, Goulet RW, Jesion G. Evaluation of a microcomputed tomography system to study trabecular bone structure. J Orthop Res 1990;8:833–42.
[78] Sedlin ED, Hirsch C. Factors affecting the determination of the physical properties of femoral cortical bone. Acta Orthop Scand 1966;37:29–48.
[79] Currey JD, Brear K, Zioupos P, Reilly GC. Effect of formaldehyde fixation on some mechanical properties of bovine bone. Biomaterials 1995;16:1267–71.
[80] Nazarian A, Hermannsson BJ, Muller J, Zurakowski D, Snyder BD. Effects of tissue preservation on murine bone mechanical properties. J Biomech 2009;42:82–6.
[81] Roberts WE, Helm FR, Marshall KJ, Gongloff RK. Rigid endosseous implants for orthodontics and orthopaedic anchorage. Angle Orthod 1989;59:247–56.
[82] Stadlinger B, Ferguson SJ, Eckels U, Mai R, Lode AT, Loukota R, et al. Biomechanical evaluation of a titanium implant surface conditioned by a hydroxide ion solution. Br J Oral Maxillofac Surg 2010;50:74–9.
[83] Gahlert M, Rohling S, Sprecher CM, Eichhorn S, Steinhäuser E, Wieland M, et al. Osseointegration of zirconia dental implants with a new rought surface. A biomechanical and histological study in mini pig. Eur Cell Mater 2008;16:34.
[84] Davison KS, Siminoski K, Adachi JD, Hanley DA, Goltzman D, Hodsman AB, et al. Bone strength: the whole is greater than the sum of its parts. Semin Arthritis Rheum 2006;36:22–31.
[85] Cha JY, Kil JK, Yoon TM, Hwang CJ. Miniscrew stability evaluated with computerized tomography scanning. Am J Orthod Dentofacial Orthop 2010;137:73–9.
[86] Bilhan H, Arat S, Geckili O. How precise is dental volumetric tomography in the prediction of bone density? Int J Dent 2012;2012:348908.